Tutorials and Reviews

International Journal of Bifurcation and Chaos, Vol. 10, No. 12 (2000) 2669–2687

NUMERICAL COMPUTATION OF CANARDS

JOHN GUCKENHEIMER
Mathematics Department, Cornell University, Ithaca, NY 14853, USA

KATHLEEN HOFFMAN
Mathematics Department, University of Maryland, Baltimore County, Baltimore, MD 21250, USA

WARREN WECKESSER
Mathematics Department, University of Michigan, Ann Arbor, MI 48109, USA

Received January 19, 2000

Singularly perturbed systems of ordinary differential equations arise in many biological, physical and chemical systems. We present an example of a singularly perturbed system of ordinary differential equations that arises as a model of the electrical potential across the cell membrane of a neuron. We describe two periodic solutions of this example that were numerically computed using continuation of solutions of boundary value problems. One of these periodic orbits contains *canards*, trajectory segments that follow unstable portions of a slow manifold. We identify several mechanisms that lead to the formation of these and other canards in this example.

1. Introduction

From the mechanics of the Van der Pol oscillator to the chemical kinetics of enzymatic reactions, singularly perturbed systems of ordinary differential equations describe complicated behavior that results from the multiple time scales in the system. Solutions of the forced Van der Pol oscillator, for example, contain such complicated phenomena as canard solutions and horseshoes. As the dimension of the systems increases, so does the complexity of the solutions. Previous work on qualitative analysis of singularly perturbed systems has focused on local phenomena within low dimensional systems. Our long-term goal is to understand and classify the local and global bifurcations that occur in these systems using the tools of geometric singular perturbation theory and asymptotic analysis. Towards that end, we have undertaken a numerical study of a system of coupled relaxation oscillators, motivated by a model of two coupled neurons.

Reciprocal inhibition of two neurons is a classical mechanism for the creation of "half center" oscillations in which there is a left–right alternation in the activity of the neurons. When one oscillator is active, the second is quiescent, and vice versa. The reciprocal inhibition prevents both oscillators from being active simultaneously. This simple network architecture is widely observed and believed to provide the neural basis of many rhythmic motions which have a bilateral symmetry in which symmetric elements act with a half period phase shift [Cohen *et al.*, 1988]. Models of varying degrees of detail for half center oscillations have been studied. Wang and Rinzel [1992] and Skinner *et al.* [1994] considered phase models in which each oscillator was represented by a single phase variable. This work introduced the concepts of "release" and "escape" and used them to understand the effects of modulatory inputs on the period of the oscillations. Nadim *et al.* [1995a, 1995b] formulated and studied much more detailed Hodgkin–Huxley like

models for the leech heart that were based upon extensive physiological data, and they compared model simulations with measurements. Here we study a model introduced by Rowat *et al.* [Rowat & Selverston, 1993; Guckenheimer & Rowat, 1997] of intermediate complexity to these two. Rowat's model represents each neuron by two variables, a membrane potential and a "recovery" variable. In this model, the periodic action potentials of an active neuron are averaged and represented by equilibria that have an elevated membrane potential relative to the membrane potential of a quiescent neuron.

Rowat's model is a singularly perturbed system with two fast and two slow variables. The membrane potentials are the fast variables while the recovery variables are assumed to change on a slower time scale. Both the relaxation of the membrane potential to an equilibrium and the response of a postsynaptic neuron to the passage of the presynaptic neuron through its threshold are fast processes. In the singular limit, the ratio of time scales becomes infinite and these models approach phase models of the type referenced above. The singular perturbation problem allows us to examine in an abstract setting the fast dynamics associated to the release and escape mechanisms. One of our objectives, only partially realized, is to characterize the dynamical events that occur at fast transitions between different states of the reciprocally inhibiting pair.

There have been few dynamical studies of the qualitative properties of singularly perturbed systems. As we demonstrate below, there are severe limitations on the capability of numerical integration to compute families of stable orbits that contain segments that are locally unstable. The locally unstable solutions are known as *canards*. Numerical integration of singularly perturbed systems with canards usually gives spurious results, producing discontinuous or chaotic transitions between stable, periodic solutions that in fact are connected by continuous families. Boundary value problem solvers that use continuation algorithms to track solutions are more successful in computing these solutions, yet present different computational challenges. The results in this paper were computed using AUTO, a widely known package for solving boundary value problems [Doedel *et al.*, 1998]. To compute solutions within specified error tolerances, we required as many as 1000 mesh intervals whereas the value recommended in the singular perturbation example of Doedel *et al.* [1998, p. 80] is 100. Moreover, it is apparent that important aspects of the solution branches computed by AUTO are not adequately resolved. In particular, we are unable to identify bifurcations of the periodic orbits or relate these to the AUTO calculation of eigenvalues for the monodromy maps of the orbits. Here we present results from our numerical study that illustrate the formation of canards of several different types, and we discuss their qualitative properties.

2. Singularly Perturbed Systems

Consider the standard form of a singularly perturbed system

$$\begin{aligned} \mathbf{x}' &= \mathbf{f}(\mathbf{x}, \mathbf{y}) \\ \mathbf{y}' &= \varepsilon \mathbf{g}(\mathbf{x}, \mathbf{y}) \,, \end{aligned} \tag{1}$$

where ε is a small parameter [Mischenko & Rozov, 1980]. Due to this small parameter, the dynamics of the variable $\mathbf{x}$ evolve on a much faster time scale than the dynamics of the variable $\mathbf{y}$. Thus, $\mathbf{x}$ is commonly referred to as the *fast variable* and $\mathbf{y}$ is called the *slow variable*. The essential idea in singular perturbation theory is to deduce the behavior of the solutions of the singularly perturbed system (1) by studying two limiting cases. The first limit $\varepsilon \to 0$ defines the *fast subsystem*:

$$\begin{aligned} \mathbf{x}' &= \mathbf{f}(\mathbf{x}, \mathbf{y}) \\ \mathbf{y}' &= \mathbf{0} \,, \end{aligned} \tag{2}$$

where the slow variables $\mathbf{y}$ are constant parameters in the vector field of the fast variable. The second limit is obtained by first rescaling time $t = \tau\varepsilon$ and then setting $\varepsilon = 0$. The resulting system is called the *slow subsystem*:

$$\begin{aligned} \mathbf{y}' &= \mathbf{g}(\mathbf{x}, \mathbf{y}) \\ \mathbf{f}(\mathbf{x}, \mathbf{y}) &= \mathbf{0} \,, \end{aligned} \tag{3}$$

a differential-algebraic system of equations. The set of equilibria of the fast system $\mathbf{f}(\mathbf{x}, \mathbf{y}) = \mathbf{0}$ is called the *critical manifold*. By combining the solutions of the fast and slow subsystems appropriately, the qualitative behavior of the singularly perturbed solution can be determined. Folds in the critical manifold correspond to saddle-node bifurcation points in the fast subsystem and are distinguished in the full system since the fundamental

nature of the solutions change at these points. Fold points correspond to points where the Jacobian $\mathbf{f_x}$ is singular. For points where $\mathbf{f_x}$ is nonsingular, the implicit function theorem can be applied so that (3) becomes $\mathbf{y}' = \mathbf{g}(\mathbf{x}(\mathbf{y}), \mathbf{y})$ and determines the dynamics of the slow subsystem.

It is a fundamental result of Fenichel [1979] that, for ε sufficiently small, a normally hyperbolic subset of the critical manifold persists as a locally invariant manifold that is $O(\varepsilon)$ close to the critical manifold. This perturbed manifold is called the *slow manifold*.

3. The Classical Canard

Special solutions to singularly perturbed systems were discovered by a group of French mathematicians using techniques from nonstandard analysis [Benoit *et al.*, 1981]. These solutions, called *canard* solutions, include segments of the solution that remain close to the unstable part of the slow manifold. The unstable nature of the canard solution combined with the fact that the solution only exists in parameter ranges that are exponentially small in relation to the small parameter ε make these solutions analytically elusive and computationally challenging. The numerical computation of these special canard solutions is the point that we address in this paper.

Consider the "classical" example of a system with canard solutions

$$\begin{aligned} \dot{x} &= \frac{y - x^2 - x^3}{\varepsilon} \\ \dot{y} &= a - x \end{aligned} \tag{4}$$

with $\varepsilon = 0.001$. The nullclines for this system are plotted in Fig. 1; the dashed and dotted lines are the x and y nullclines, respectively. In this case, the critical manifold is the x nullcline $y = x^3 + x^2$. This system undergoes a Hopf bifurcation when $a = 0$, and as a decreases, a family of periodic orbits grows out of the origin. This is a family of canard solutions; the orbits travel down the right side of the x-nullcline, and then continue *up* the unstable part of the x nullcline before jumping to the right. The distance for which the orbits track the unstable slow manifold increases, up to where the orbit reaches the local maximum in the nullcline. As a decreases further, the distance for which the orbit follows the unstable slow manifold decreases, but now the orbit jumps *left* (i.e. x jumps down in value) to the left-most stable branch of the slow manifold. Eventually, the canard disappears, and the periodic orbit becomes the standard relaxation oscillation.

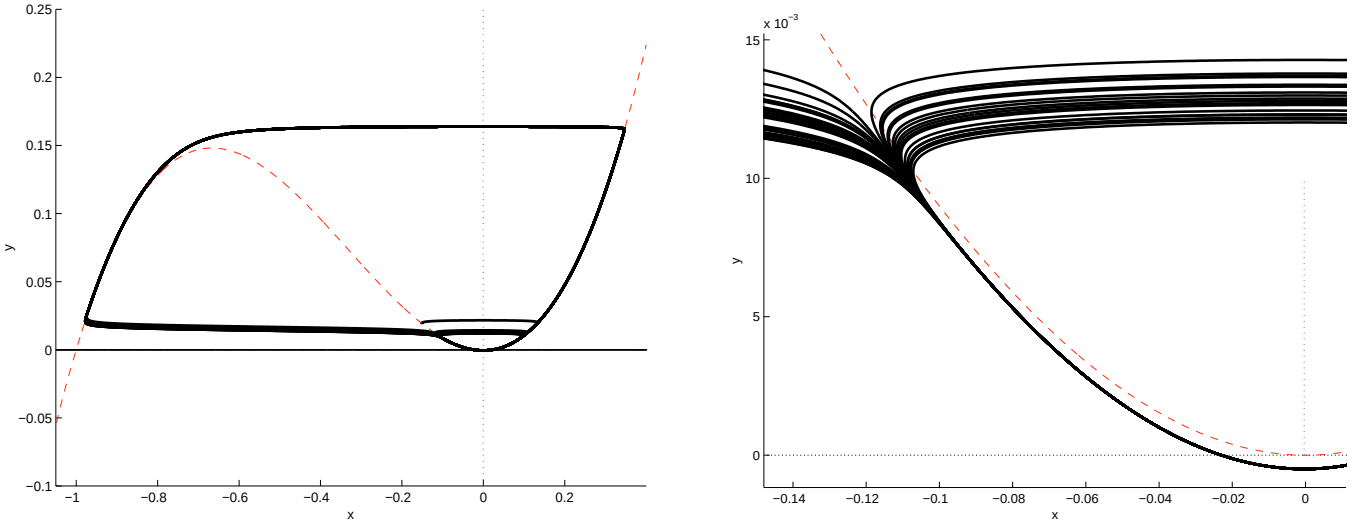

(a) (b)

Fig. 1. A numerically computed solution to Eq. (4) ($a = -3.7757344 \times 10^{-4}$). The right figure is a closer look at the region where the canard leaves the unstable part of the slow manifold. The numerical algorithm produces trajectories that jump erratically left and right from the unstable part of the slow manifold rather than clearly tracking the stable periodic orbit with a canard. This solution was computed using the MATLAB subroutine ODE15S, with error tolerances set to 10^{-11}.

Computation of the canards of this system with numerical integration fails completely. The Jacobian of the vector field is

$$\begin{pmatrix} 1000(-2x - 3x^2) & 1000 \\ -1 & 0 \end{pmatrix}.$$

We consider $-1 \ll a < 0$. On the critical manifold for $x \in [-1/2, -1/6]$, the x components of nearby trajectories separate at a rate at least $\exp(250t)$. The equations for the slow subsystem reduces to $\dot{x} = -1/(2 + 3x)$ (taking $a = 0$), and we find that a trajectory requires at least time $1/3$ to traverse the portion of the critical manifold where $-1/2 < x < -1/6$. During this time, the relative separation of trajectories in the x direction increases by a factor of well over $\exp(80)$. Thus, an initial condition must have an accuracy of at least $\exp(-80)$ close to the slow manifold to be able to track it with a numerical integration algorithm. Consequently, initial conditions that differ by unit precision but lie on opposite sides of the unstable portion of the slow manifold separate without tracking the unstable slow manifold very far. Standard numerical integration algorithms, when applied to the initial value problem, produce "chaotic" trajectories that jump erratically left and right on subsequent returns to the unstable slow manifold rather than giving a good representation of a periodic orbit with a canard. An example is shown in Figs. 1 and 2.

In contrast, boundary value problem solvers that use continuation methods are able to track canard solutions. To illustrate this point, we use AUTO [Doedel *et al.*, 1998] to track canard solutions of a system of singularly perturbed ordinary differential equations with two fast variables and two slow variables. As we will demonstrate, this particular system is much more complicated than Eq. (4) and includes canards qualitatively different from those found in (4).

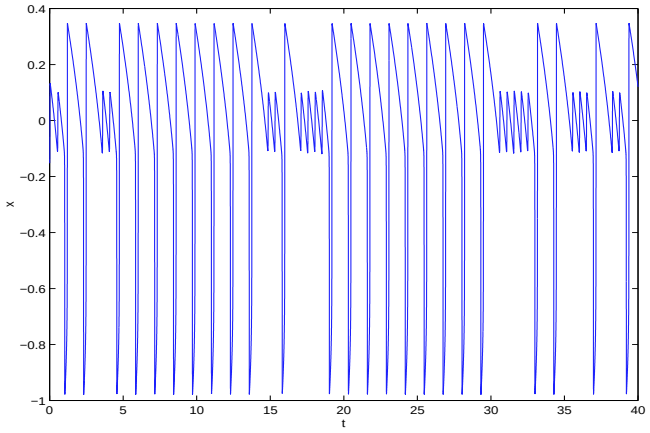

Fig. 2. A plot of the fast variable x of (4) versus time demonstrates the erratic behavior of the solution illustrated in Fig. 1.

More specifically, we demonstrate two additional classes of canards that we have observed, distinct from the classical canard described above. The first type of canard that we observed enters the unstable part of the slow manifold at a fold, a point that is not normally hyperbolic. In the fast subsystem, this corresponds to a trajectory entering a saddle-node (degenerate) equilibrium. We call this a *fold initiated canard*. For such a canard to form, the vector field on the critical manifold near the fold must point *away* from the fold.

The second class of canards occurs when the slow manifold is of saddle type (i.e. has stable and unstable fibers), and a trajectory enters the slow manifold along a stable fiber. In the fast subsystem, this trajectory is the stable manifold of a saddle. We call this a *saddle initiated canard*. Note that this type of canard can only occur in systems with at least two fast variables.

4. The Model

4.1. *The equations*

The Hodgkin–Huxley equations [Hodgkin & Huxley, 1952], a widely accepted model for the voltage potential in a squid giant axon, is a well-known system of mildly stiff ordinary differential equations. Instead of trying to understand a model with the complexity of the Hodgkin–Huxley equations, we study a simpler model of two coupled neurons that does not attempt to resolve individual conductances within the membranes of the neurons. The particular model that we studied was formulated as a description of neurons coupled with reciprocal inhibition in the gastric mill circuit of a lobster [Guckenheimer & Rowat, 1997; Rowat & Selverston, 1993]. Specifically, the model is

$$\begin{aligned} v_1' &= -\left(v_1 - a\tanh\left(\frac{\sigma_1 v_1}{a}\right) + q_1 + \omega f(v_2)(v_1 - r)\right) \\ v_2' &= -\left(v_2 - a\tanh\left(\frac{\sigma_2 v_2}{a}\right) + q_2 + \omega f(v_1)(v_2 - r)\right) \\ q_1' &= \varepsilon(-q_1 + s v_1) \\ q_2' &= \varepsilon(-q_2 + s v_2)\,, \end{aligned} \tag{5}$$

where the fast variables v_k represent the membrane potential and the slow variables q_k represent the idealized gating of the membrane channels. We assume that the two neurons are coupled by a function of the form $\omega f(v_j)(v_i - r)$ where $f(x)$ is given by

$$f(x) = \frac{1.0}{1.0 + \exp(-4\gamma(x - \theta))} \tag{6}$$

and the parameter ω controls the coupling strength. The parameter γ governs the steepness of the threshold for synaptic coupling. We take $\gamma = 10$, a value large enough to produce a steep threshold between minimal and maximal synaptic current. We take the small parameter ε to be $\varepsilon = 0.0001$.

From a different perspective, Eq. (5) also represents two "oscillators" (v_1, q_1) and (v_2, q_2) coupled by the function (6). When isolated ($\omega = 0$), each oscillator has parameter ranges in which it is bistable, that is it has two stable equilibria. The equilibria of an isolated neuron with larger values of v_i represent states in which the neuron fires periodic action potentials. The oscillations associated with these periodic states are averaged, however. More complete models of reciprocal inhibition include the spiking action potentials of the active state [Nadim *et al.*, 1995a].

We assume that the oscillators are identical, that is, the parameters for each oscillator are the same, with the exception of σ, the parameter which controls the steepness of the tanh function. The value of the remaining parameters are:

$$\begin{aligned} &\omega = 0.03, && \gamma = 10, && r = -4\,, \\ &\theta = 0.01333, && a = \ \ 1, && s = 1\,. \end{aligned} \tag{7}$$

4.2. *Fast and slow subsystems*

To understand the qualitative features of the solutions of (5), we describe our numerically computed solutions to the full singularly perturbed system in terms of the singular solutions of the fast and slow subsystems [Arnold *et al.*, 1994; Guckenheimer & Holmes, 1983; Jones, 1994; Kevorkian & Cole, 1981; Mischenko & Rozov, 1980]. The fast subsystem is

$$\begin{aligned} v_1' &= -\left(v_1 - a\tanh\left(\frac{\sigma_1 v_1}{a}\right) + q_1 + \omega f(v_2)(v_1 - r)\right) \\ v_2' &= -\left(v_2 - a\tanh\left(\frac{\sigma_2 v_2}{a}\right) + q_2 + \omega f(v_1)(v_2 - r)\right) \end{aligned} \tag{8}$$

where the slow variables, q_1 and q_2, act as parameters. The slow subsystem is given by

$$\begin{aligned} q_1' &= (-q_1 + s v_1) \\ q_2' &= (-q_2 + s v_2)\,, \end{aligned} \tag{9}$$

$$\begin{aligned} &-\left(v_1 - a\tanh\left(\frac{\sigma_1 v_1}{a}\right) + q_1 + \omega f(v_2)(v_1 - r)\right) = 0 \\ &-\left(v_2 - a\tanh\left(\frac{\sigma_2 v_2}{a}\right) + q_2 + \omega f(v_1)(v_2 - r)\right) = 0 \end{aligned} \tag{10}$$

where the algebraic Eqs. (10) define the critical manifold.

To understand the solutions to the full singularly perturbed system (5) we use information from the fast subsystem (8) and the slow subsystem (9) and (10). We begin by studying folds in the critical manifold. Folds in the critical manifold occur where the Jacobian of (10) with respect to the fast variables $\mathbf{v} = (v_1, v_2)$ is singular. Specifically

$$\det(\mathbf{f}_{\mathbf{v}}) = 0\,, \tag{11}$$

where Eq. (10) defines $\mathbf{f}(\mathbf{v}, \mathbf{q})$. Thus the solutions (v_1, v_2) to (11) define the curve of fold points on the critical manifold. The projection of these fold lines on the slow variables (q_1, q_2) is given by substituting the solutions (v_1, v_2) into (10) and solving for the corresponding pair (q_1, q_2).

The fold lines of the critical manifold determine possible points at which the solution will either leave the neighborhood of the slow manifold and begin a fast transition or form a fold initiated canard. The points along the fold lines at which a fold initiated canard is possible are determined by the dynamics on the critical manifold near the fold line. Although the slow dynamics are typically defined in terms of the slow variable $\mathbf{q}$ (as described in the introduction), we express the slow dynamics in terms of the fast variables as a matter of convenience. Equation (10) can easily be solved for $\mathbf{q} = \hat{\mathbf{f}}(\mathbf{v})$, whereas solving $\mathbf{v} = \mathbf{g}(\mathbf{q})$ is much more difficult.

To determine the dynamics near a fold in the critical manifold, we consider the vector form of Eqs. (9) and (10):

$$\begin{aligned} \mathbf{q}' &= \mathbf{g}(\mathbf{v}, \mathbf{q})\,, \\ \mathbf{f}(\mathbf{v}, \mathbf{q}) &= \mathbf{0}\,. \end{aligned} \tag{12}$$

The implicit function theorem can be applied to solve $\mathbf{f}(\mathbf{v}, \mathbf{q}) = \mathbf{0}$ for $\mathbf{q}$ as a function of $\mathbf{v}$. Then Eq. (9) becomes

$$\mathbf{v}' = (\hat{\mathbf{f}}_{\mathbf{v}})^{-1}\mathbf{g}(\mathbf{v}, \hat{\mathbf{f}}) = \frac{\operatorname{adj} \hat{\mathbf{f}}_{\mathbf{v}}}{\det \hat{\mathbf{f}}_{\mathbf{v}}}\mathbf{g}(\mathbf{v}, \hat{\mathbf{f}}), \tag{13}$$

where $\hat{\mathbf{f}}$ is defined by the relation $\mathbf{q} = \hat{\mathbf{f}}(\mathbf{v})$. The vector field defined in (13) becomes singular at the fold since $\det \hat{\mathbf{f}}_{\mathbf{v}} = 0$ along the fold. To circumvent this singularity, we multiply the right-hand side of the equation by $\det \hat{\mathbf{f}}_{\mathbf{v}}$, a scalar quantity that will change the length of the vector field, and possibly the sign of the vector field. But by calculating the sign of $\det \hat{\mathbf{f}}_{\mathbf{v}}$ independently, we will know the direction of the vector field at a fold. Note that $\mathbf{q}$ can be recovered from the relation $\mathbf{q} = \hat{\mathbf{f}}(v_1, v_2)$.

5. Computation of Solutions

Our primary tool for numerically computing families of periodic orbits was the continuation package AUTO [Doedel *et al.*, 1998]. AUTO uses collocation to solve the boundary value problem associated with finding a periodic orbit. Because we are computing fairly complicated periodic orbits in a system with widely different time scales, it was necessary to use as many as 1000 mesh points and error tolerances as low as 10^{-10}. (This may be compared to the singular perturbation example given by Doedel *et al.* [1998], where only 100 mesh points were used with error tolerances of 10^{-6}.) The average time for AUTO to compute 1000 periodic solutions on an SGI Challenge L with 4 R10,000-195 MHz CPUs and 2 Gigabytes of four-way interleaved memory was 45 minutes.

To compute a starting solution for the continuation algorithm, we solved the system using a numerical initial value problem solver, with a set of parameters for which the computed trajectory approaches a periodic orbit with no canards. We used the MATLAB function ODE15S, an adaptive algorithm designed for stiff systems, to solve the differential equations. To obtain accurate results, we used error tolerances as low as 10^{-9}. For large ranges of the parameter σ_2, the system converges to a stable periodic orbit. We used orbits computed this way as starting points in AUTO. Additionally, we used MATLAB to plot and animate the solutions generated by AUTO.

Because our system of equations is four-dimensional, visualization of the phase space is problematic. We plot an assortment of projections to do so. The two-dimensional projections that we have found most useful are the fast variables (v_1, v_2), the first oscillator (v_1, q_1), and the second oscillator (v_2, q_2). Occasionally it is also helpful to see three-dimensional projections, so in some cases we plot (v_1, v_2, q_1) and (v_1, v_2, q_2).

The parts of the solution where the speed of the trajectory is much greater than ε (which for our computations is 10^{-4}) are called "fast transitions"; these are the parts where the fast subsystem provides a good approximation to the full system. When a trajectory slows down to $O(\varepsilon)$, the fast subsystem is no longer a good approximation; the "fast" variables are now changing on the same time scale as the slow variables. In this case, the slow subsystem (i.e the dynamics on the critical manifold) provides a good approximation to the solution, and we will often say that the trajectory is "on the slow manifold". In the plots of solutions (such as Fig. 3), the slow parts are plotted with thick (blue) lines, and the fast transitions are plotted with thinner (red) lines. Whether a part of the solution is considered slow or fast in these plots is decided by computing the norm of the vector field. If it is above an arbitrary threshold, it is called fast; otherwise it is slow.

We begin by describing in Sec. 5.1 one of the simpler solutions of (5) that represents two symmetric oscillators. This example provides a basis for introducing the projections and the terminology with which we describe the behavior of the solutions. With this foundation, we present in Sec. 5.2 a more complicated asymmetric solution containing three canards.

5.1. *Symmetric oscillators*

Models of symmetrically coupled reciprocally inhibited identical neurons such as (5) produce "half-center" oscillations in which the two neurons oscillate half a period out of phase of each other. There is a symmetry of the orbits corresponding to interchange of the two neurons and advancing time of a half period. While one neuron is active, the other is quiescent. We begin by presenting a solution of (5) which exhibits this behavior. This will illustrate the two-dimensional and three-dimensional projections of trajectories in the context of a simple and familiar example.

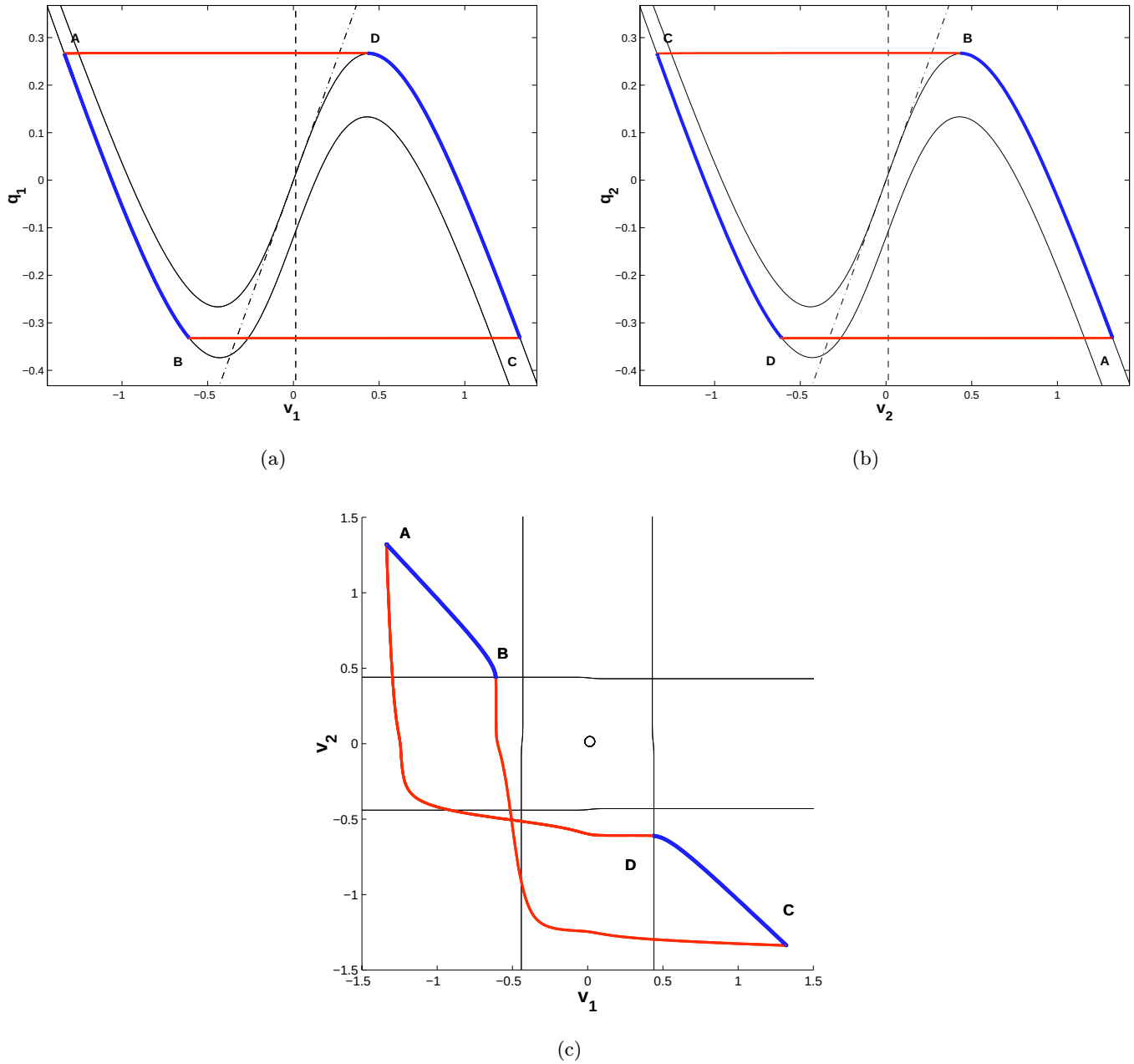

(a) (b)

(c)

Fig. 3. Three two-dimensional projections of the periodic solution of the symmetric oscillators that exhibit half-center oscillations are portrayed in this figure. The phase portraits of the oscillators (v_1, q_1) and (v_2, q_2) depict the slow segments of the orbit (thick solid blue lines) and fast segments of the orbit (thick solid red lines) as well as the q_i-nullclines (dot–dashed line), the upper and lower bounds of the v_i-nullclines (thin solid line), and the v_i-threshold (vertical dashed line). The (v_1, v_2) projection of the solution also contains the fold lines, as defined by Eq. (11).

Consider the model (5) with the parameter values given by Eq. (7) and $\sigma_1 = \sigma_2 = 2$. The stable periodic solution that exhibits half-center oscillations is depicted in Figs. 3–5. In Fig. 3, three two-dimensional projections of the solution are shown. The plots of the solution projected onto the fast variables (v_1, v_2) [Fig. 3(c)] also contain the projections of the fold curves of the slow manifold [computed by solving Eq. (11)] plotted as thin solid curves. Note that the changes in speed of the orbit occurring at B and D correspond to the orbit leaving the slow manifold at a fold and beginning a fast transition to another part of the slow manifold. Compare also Fig. 5 where the jumps of

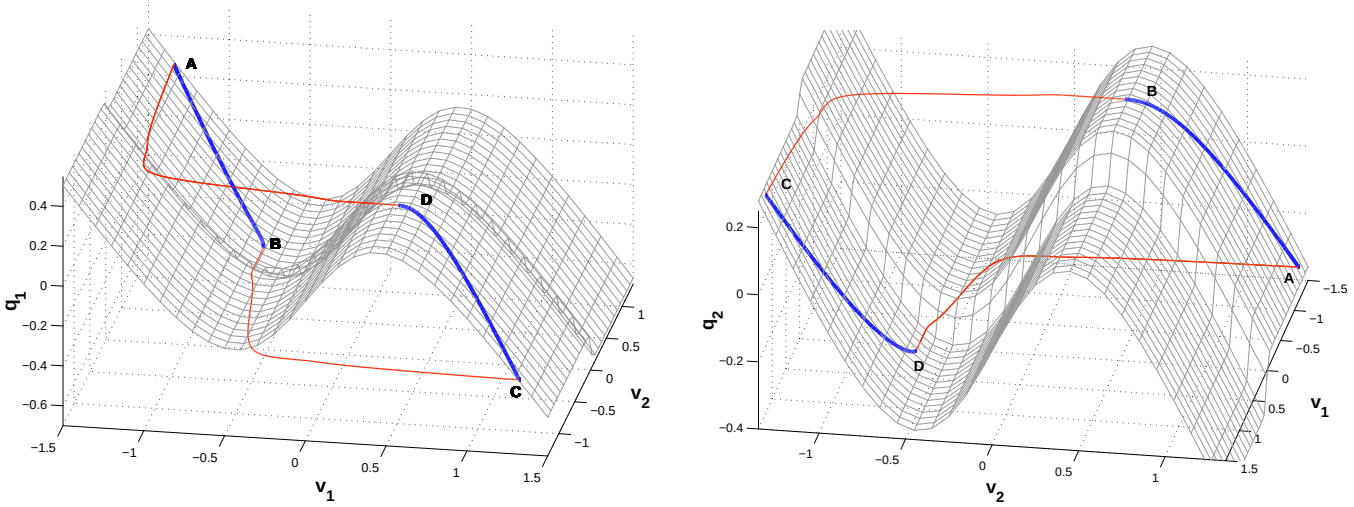

(a) (b)

Fig. 4. Two three-dimensional views of the critical manifold and the periodic solution of the symmetric system give a different perspective on the solution.

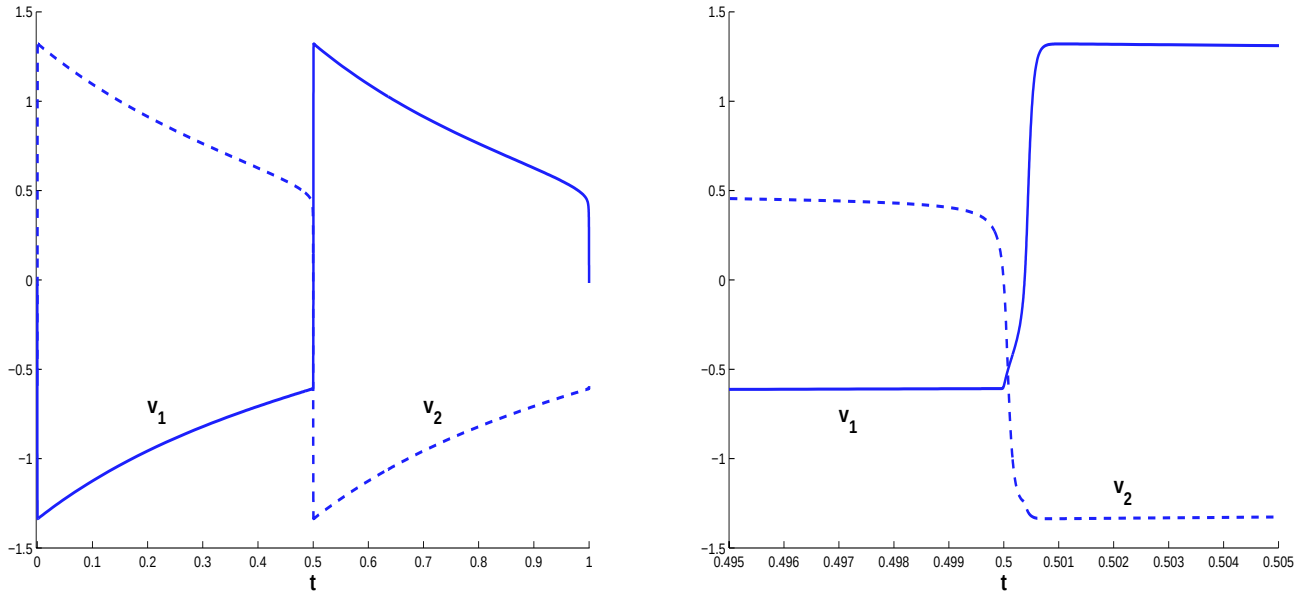

(a) (b)

Fig. 5. The voltage of each oscillator is plotted against time t for the periodic solution to the symmetric system. The voltage potential of the first oscillator v_1 represented by the solid line and v_2 is represented by the dashed line.

v_i occur simultaneously at times 0% and 50% of the period.

Figures 3(a) and 3(b) show the "phase plane" associated with each of the oscillators. Each plot includes the q_i-nullcline (dot–dashed line), the v_i threshold (vertical dashed line), and the projection of the periodic orbit. In addition, the plots contain the upper and lower limits of the v_i-nullcline (thin solid lines). The lower limit of the v_i-nullcline corresponds to the value of the coupling function being zero, which occurs when the voltage of the other oscillator is sufficiently below the threshold θ. Analogously, the upper limit corresponds to the value of the coupling function being one, which occurs when the voltage of the other oscillator is sufficiently above the threshold θ. When the voltage

of the other oscillator is in a neighborhood of the threshold θ, the value of the coupling function is between zero and one and the v_i-nullcline is between the upper and lower limits.

Figures 4(a) and 4(b) are three-dimensional plots of the periodic orbit in (v_1, v_2, q_1) coordinates and (v_1, v_2, q_2) coordinates, respectively. These plots include the two-dimensional critical manifold.

The following detailed description of the periodic orbit refers to Figs. 3–5. At point A, the orbit has just completed a fast transition; in the fast subsystem, this means that the orbit has entered a small neighborhood of a critical point of the fast subsystem, which in this case is a stable node. The orbit then moves along the slow manifold from A to B. In Fig. 3(a), the segment from A to B is close to the lower v_1-nullcline. Because v_1 is to the left of the v_1 threshold [as shown by the vertical dashed lines in Fig. 3(a)], v_2 is on its upper nullcline, and similarly v_1 is on the lower nullcline because v_2 is above threshold. At B, the orbit reaches a fold in the slow manifold. This can be seen in Fig. 3(b), where we see that the slow segment ends at the knee (i.e., local maximum) of the upper v_2-nullcline. In Fig. 3(c), we see that B is the intersection of the trajectory and a fold line; in Fig. 4(b), it is clear that B is at the fold in the slow manifold. A fast transition begins at B. In Fig. 3(b), the fast transition is a jump down (to the left). During this jump, v_2 crosses threshold, which moves the v_1-nullcline up towards its upper limit. When this happens, the first oscillator is no longer near its nullcline, and it begins a fast jump up (to the right). In the terminology of Skinner *et al.* [1994], the first oscillator has been "released". As it jumps, it crosses the threshold for activating its synaptic inhibition of the second oscillator. Thus the point C lies on the lower nullcline for v_2. Both oscillators cross their threshold in the transition from B to C, the first oscillator turning on its inhibition of the second oscillator while the second oscillator turns off its inhibition of the first oscillator. Because the oscillators are symmetric, the transitions C $\to$ D $\to$ A are the same as A $\to$ B $\to$ C, but with the roles of the oscillators reversed.

5.2. *Asymmetric oscillators*

The symmetric solution presented in Sec. 5.1 is a stable periodic orbit with no canards. It can be computed quite easily by letting a standard numerical differential equation solver integrate forward in time until a given convergence criterion is reached. As we track one parameter families of periodic orbits to the system (5), allowing the parameter σ_2 to vary, canards appear and disappear in the periodic orbits. The occurrence of canards makes computing periodic orbits more difficult. We saw in Sec. 3 that when a periodic orbit has a canard, using an initial value problem solver has severe limitations, even if the orbit is stable. The degeneracies of the slow–fast system associated with the formation of canards are discussed in Sec. 6. In this section, we describe a single periodic orbit that illustrates the complexity of the solutions to Eq. (5). We also note that this complexity seems to be beyond that which has been achieved previously in computations with AUTO. The example we display has parameters $\sigma_1 = 3$ and $\sigma_2 = 1.2652372051$. Figures 6–8 show a periodic orbit computed by AUTO at these parameter values. This example contains one fold initiated and two saddle initiated canards.

To understand the structure of this trajectory and how it interacts with the slow manifold, we give a detailed description of the periodic orbit, beginning at the point labeled A. In the symmetric half-center oscillations, the interaction between the two oscillators can be easily characterized. When the first oscillator is on its lower (upper) nullcline, the second oscillator is on its upper (lower) nullcline. The solution presented in Figs. 6–8 shows a much more complicated interaction between the oscillators. Beginning at the point labeled A, the first oscillator makes a series of jumps between its upper and lower nullclines without crossing its synaptic threshold (depicted by the vertical dashed line), so the second oscillator remains on its upper nullcline in a typical relaxation oscillation pattern. In contrast to the symmetric solution, in this example both oscillators can be on their upper nullcline at the same time! An analogous situation exists as the first oscillator jumps between its upper and lower nullclines as it proceeds from point C to the maximum of the lower nullcline. The first oscillator is always above its threshold, thus the second oscillator remains on its lower nullcline.

For generic trajectories, stable segments of slow motion in the system terminate near fold points of the critical manifold or near points of Hopf bifurcation. Thus the location of folds is closely related to the initiation of canards. In this system, the folds lie close to the local minima and maxima of the v-nullclines in the plane of each oscillator, except

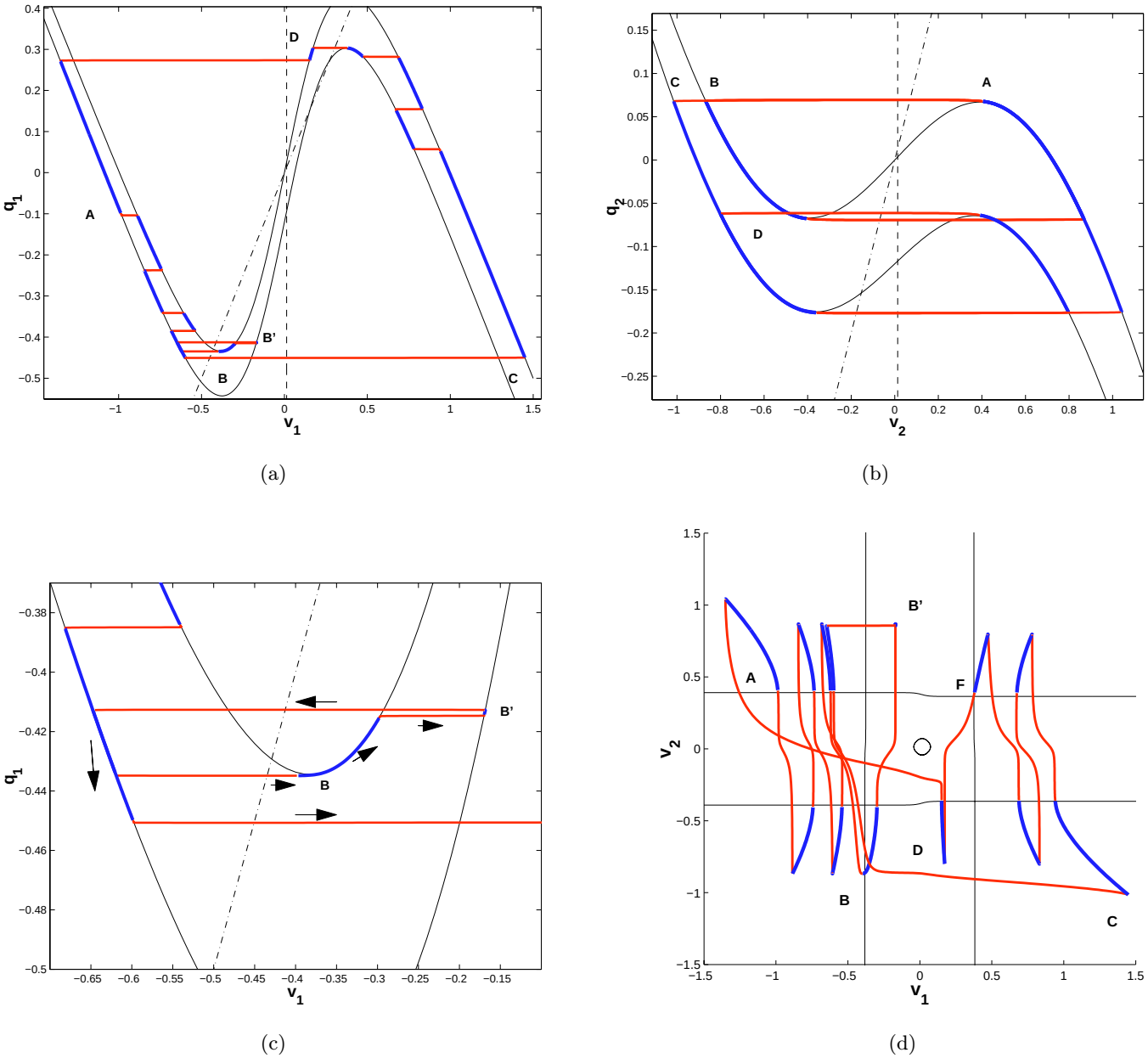

Fig. 6. Complicated periodic orbit computed by AUTO for asymmetric oscillators. The upper figures depict the phase plane for (a) the first oscillator and (b) the second oscillator. (c) The bottom left figure is a blowup of the local minimum of the nullcline of the first oscillator shown in the upper left. (d) The bottom right figure depicts the projection of the solution onto the fast variables.

when the other oscillator is at its synaptic threshold. We locate fold initiated canards visually by looking for points of tangency between the projection of a trajectory into the plane of one of the oscillators and the v-nullcline in that plane. Our example periodic orbit contains one fold initiated canard at the point labeled B. As can be seen in Fig. 6(c), the first oscillator makes a fast transition from its lower nullcline to a minimum of its upper nullcline. (This corresponds to a trajectory encountering a saddle-node point in the fast subsystem.) At this point, labeled B, the orbit proceeds up the unstable portion of the slow manifold (corresponding to saddles in the fast system). This is a *fold initiated* canard. At the next fast transition, the first oscillator leaves the unstable portion of its upper nullcline, follows the stable manifold of another saddle (in the fast subsystem) to the unstable lower

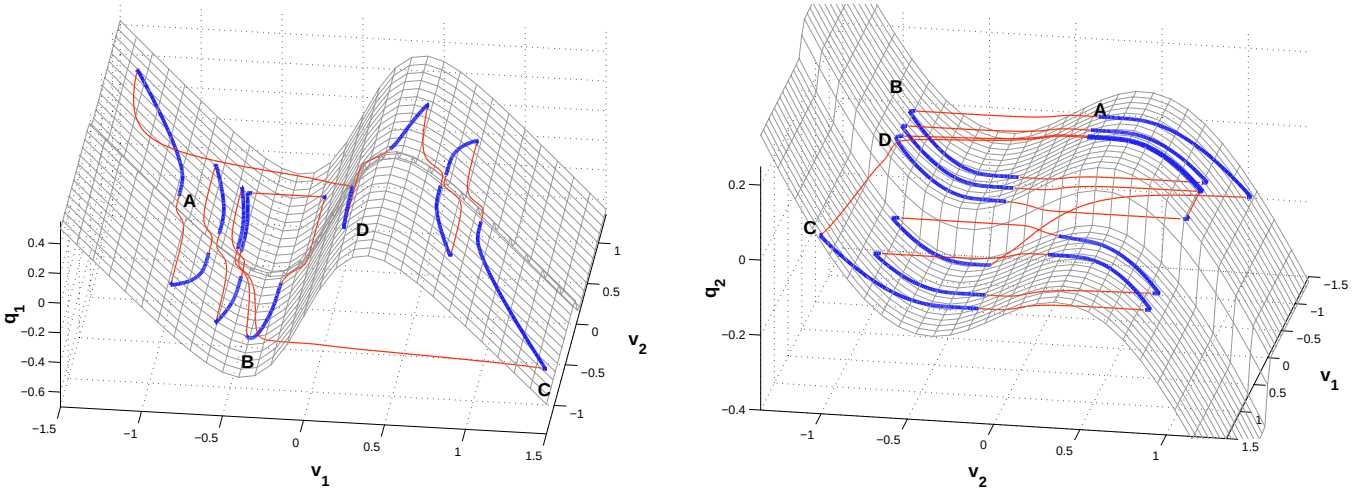

(a) (b)

Fig. 7. Three-dimensional views of the asymmetric periodic orbit. These figures include the two-dimensional critical manifold, and show that the orbit tracks the slow manifold when the trajectory is moving slowly (thick intervals of the curve). The canards are visible in the figure on the left; they are the thick parts of plotted trajectory that track the slow manifold in the region $-0.5 < v_1 < 0.5$ (between the lower fold and the upper fold).

nullcline at B' and a *saddle initiated* canard is born. This brief canard ends when the trajectory leaves the saddle, and in the subsequent fast transition, v_1 decreases while v_2 remains approximately constant. This part of the orbit is the horizontal segment in the upper part of the (v_1, v_2) projection shown in Fig. 6(d) with $v_2 \approx 0.9$. Next, there is a slow transition to a fold of the second oscillator. In the subsequent fast transition, the trajectory misses the fold

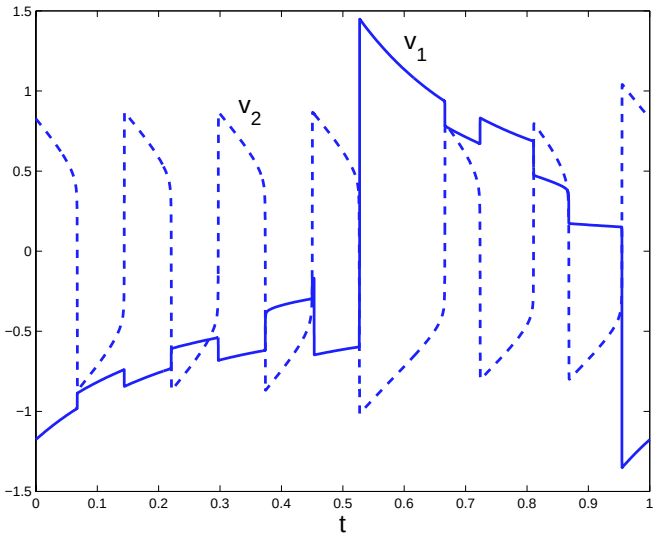

Fig. 8. Complicated periodic orbit computed by AUTO for asymmetric oscillators. This orbit has three canards.

of the first oscillator on the upper nullclines and continues on to the point labeled C, where the oscillations described in the previous paragraph continue. A second *saddle initiated* canard is formed as the first oscillator leaves the maximum of its lower nullcline and is drawn in along the stable manifold of a saddle in the fast subsystem to the unstable part of the upper nullcline at point D. As the orbit leaves this saddle initiated canard, the first oscillator crosses threshold, thus forcing the second oscillator to jump to its upper nullcline. The next fast transition occurs at the initial point A where the second oscillator reaches the local maximum of its upper nullcline. We have returned to the initial point of the periodic orbit.

Prior to the formation of the saddle initiated canard at the point labeled D, the trajectory crosses the fold curves of both oscillators almost at the same time. This point labeled F is seen in Fig. 6(d), the (v_1, v_2) projection at the upper right intersection of the two fold curves. Our description of the dynamics obscures some of the detail associated with the fold surfaces of the four-dimensional coupled system. One aspect of this model is that the synaptic conductance term through which the two oscillators are coupled is almost constant except at the synaptic threshold. Away from the synaptic threshold, the critical surface of the coupled system is approximated by products of the critical curves

of each oscillator (in its inhibited or uninhibited state depending upon whether the other oscillator is above or below synaptic threshold). The fold curves of the coupled system are approximately products of the fold points of one oscillator with the critical curve of the other. This is what we have displayed in our figures. The resulting self intersections of the approximate fold curves are degenerate singularities that we call double folds. For a generic mapping, we expect to encounter only folds and cusps as singularities of the projection of the critical manifold onto the plane of the fast variables, not double folds [Arnold, 1968]. The flow near a double fold point is the product flow of two saddle-nodes. It has a quadrant of trajectories that flow into the double fold point and a quadrant of trajectories that leave the double fold point. Thus we should not be surprised to see a trajectory that encounters the intersection point of the two fold curves. Guckenheimer and Khibnik [1997] have analyzed the bifurcations of two weakly coupled oscillators, showing how the dynamics of uncoupled oscillators perturb with weak coupling. We have not attempted here to resolve details of the dynamics of the frozen system ($\varepsilon = 0$) near the intersection points of the fold curves.

6. Formation of Canards

We have displayed three different types of canards:

- "classical" canards associated with Hopf bifurcation
- fold initiated canards that occur as a fast trajectory approaches a critical manifold near a fold point
- saddle initiated canards that occur when a fast trajectory approaches the critical manifold along the stable manifold of a saddle point.

In this section, we present numerical examples that illustrate the *formation* of each type of canard in the system (5). We show one additional type of classical canard, initiated by the appearance of a "folded saddle" [Arnold *et al.*, 1994] rather than a Hopf bifurcation. We demonstrate intermediate stages of the processes that create each type of canard as a parameter or initial point varies. Illustrations of the evolution of classical and fold initiated canards can be found in [Diener, 1984] and [Arnold *et al.*, 1994].

6.1. *Classical canards*

As was discussed in Sec. 3, there is a family of periodic orbits for the system (4), parametrized by a, that is born in a Hopf bifurcation and ultimately becomes a relaxation oscillation. The Hopf bifurcation and relaxation oscillations occur on opposite sides of the critical manifold. As the periodic solutions grow, they cross the critical manifold by developing segments that lie along the unstable portion of the slow manifold. These are canards. The properties of these canards have been analyzed in great detail from multiple perspectives [Diener, 1984; Dumortier & Roussarie, 1996; Eckhaus, 1983]. The salient features of the "classical" asymptotic analysis are that

- The canards occur at parameter values comparable to ε.
- The parameter interval during which the canards occur has a length comparable to $\exp(-c/\varepsilon)$ with c a positive constant that has been explicitly computed.
- There are asymptotic expansions for the canards and the parameter values at which they occur.
- As $\varepsilon \to 0$, the canards approach closed curves formed from segments of the slow and fast vector fields.

Hopf initiated canards can occur in systems with one slow and one fast variable as illustrated by the system (4). The periodic orbits of (5) that we have exhibited thus far are not close to Hopf bifurcations. We have numerically investigated some Hopf bifurcations that occur in (5), and they exhibit the same qualitative behavior as those (4). For example, Fig. 9 shows solutions (in the (v_2, q_2) plane) from a family of periodic orbits that arise from a Hopf bifurcation that occurs when $(\sigma_1, \sigma_2) = (3, 2.7338807152)$. As predicted by the asymptotic analysis of the Hopf canards, the periodic orbits grow in amplitude very quickly at some distance from the Hopf bifurcation itself.

6.1.1. *Classical canard (second example)*

This example shows the formation of a canard by passage through a folded saddle. The smallest dimension in which folded saddles occur is in systems with two slow variables and one fast variable. At typical fold points of a generically perturbed system, trajectories on the critical manifold approach the fold from both sheets or they leave the fold from

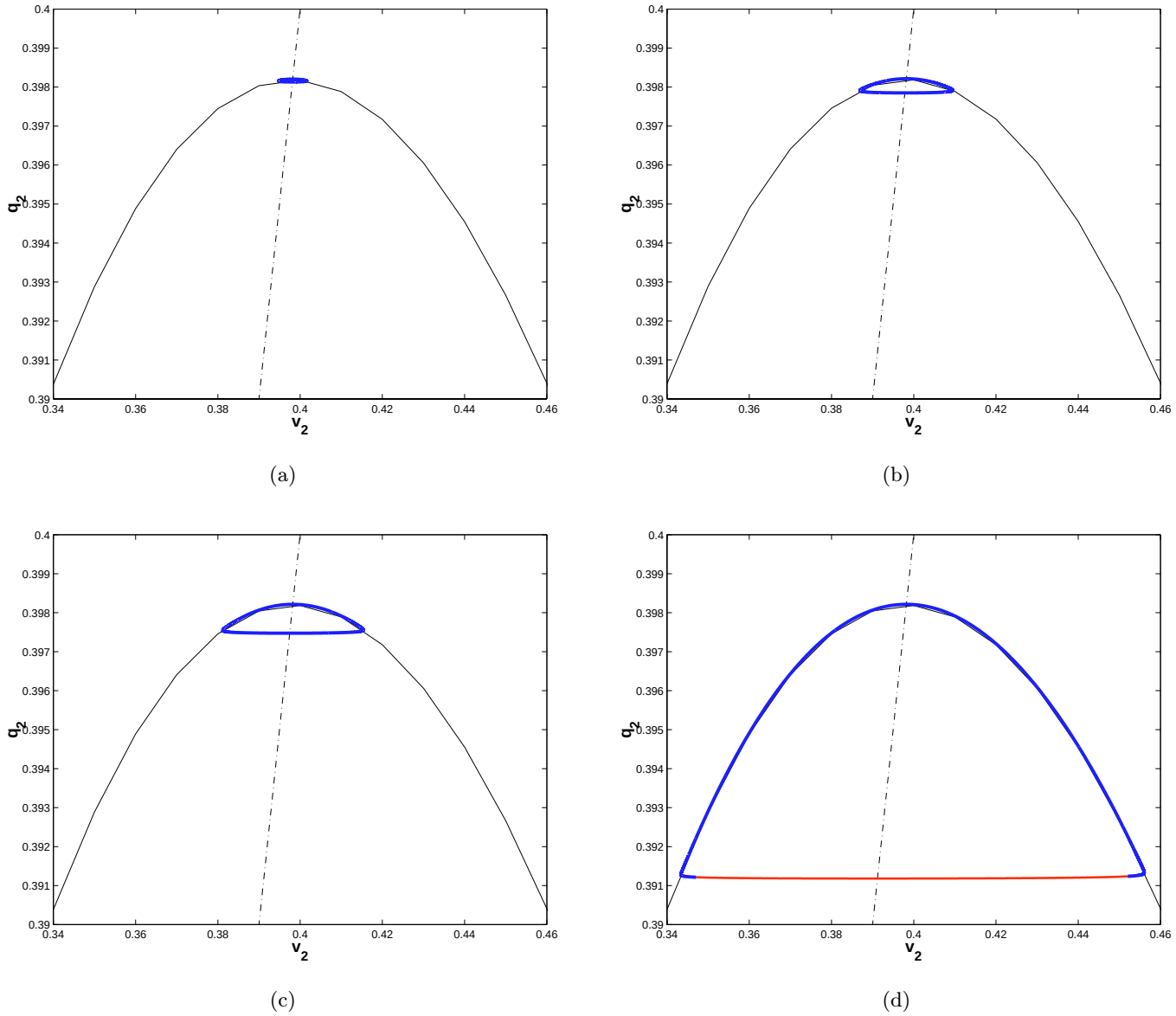

(a) (b)

(c) (d)

Fig. 9. This sequence of plots shows the periodic orbits that arise from a Hopf bifurcation.

both sheets. At isolated points of a fold curve in a generic system with two slow variables, equilibrium points may be encountered [Arnold *et al.*, 1994]. When this happens, the trajectories on the critical manifold approach the fold curve on one side of the equilibrium point and leave the fold curve on the other side of the equilibrium point. In the slowly varying system, some trajectories may have extensions that go through the fold while remaining close to the critical manifold. These are classical canards in that the trajectory tracks a critical manifold through a fold as do the Hopf initiated canards. We call these canards equilibrium point initiated canards.

Figure 10 shows the relevant details of a solution with an equilibrium point initiated canard. There is one aspect of this example that differs a bit from other examples that we present, namely that the canard formation itself takes place along a canard. The incoming trajectory to the fold curve lies along a portion of the slow manifold with one unstable direction, and the outgoing trajectory lies along a portion of the slow manifold with two unstable directions. The three panels of the figure show the projection of segments of three solutions onto the plane of the second oscillator. Not shown in the figure, the projection of this trajectory segment onto the plane of the first oscillator lies near the

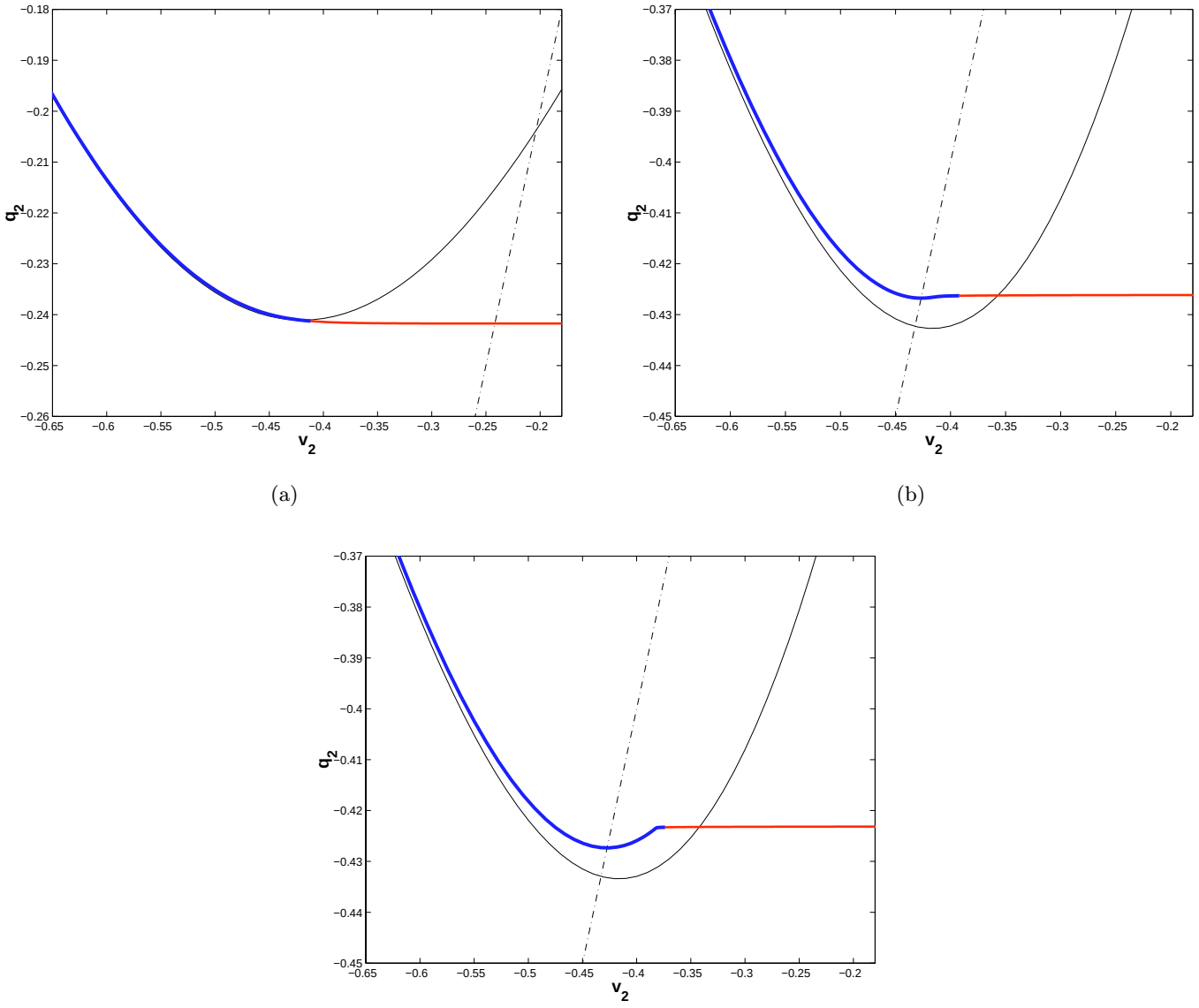

Fig. 10. (a) The first plot illustrates a regular jump off a fold. (b) The second plot shows the q_2-nullcline is very close to the fold, and a canard is beginning to form, and in (c) there is a longer canard.

unstable branch of the v_1-nullcline. As the parameter σ_2 varies, v_1 approaches its synaptic threshold from above during the slow motion. This causes the inhibition of the second oscillator to diminish and raises the v_2-nullcline. Only the lower limit of the v_2-nullclines corresponding to full inhibition from the first oscillator is shown in the figure. The equilibrium point initiated canard occurs as an equilibrium point approaches a fold point of the critical manifold. This equilibrium point is called a folded saddle. The figure displays the q_2-nullcline as well as the lower limit of the v_2-nullclines. When the q_2- and v_2-nullclines cross near the local minimum of the v_2-nullcline, the system is close to the folded saddle point where the equilibrium point initiated canard occurs.

6.2. *Fold initiated canards*

A fold initiated canard occurs when a fast transition passes through a neighborhood of a saddle-node point for the fast subsystem, leaving this neighborhood along a branch of unstable points in the slow manifold. Recall that saddle-node points of the fast

subsystem are fold points of the critical manifold. At generic fold points, the flow either

- approaches the fold from both sheets of the slow manifold resulting in a fast jump, or
- leaves the fold on both sheets of the slow manifold.

The fold initiated canards occur in the second case. The essential properties of the fold initiated canard occur already in systems with one fast and one slow variable. The system of equations

$$\begin{aligned} \dot{x} &= -y + x^2 \,, \\ \dot{y} &= \varepsilon \end{aligned} \tag{14}$$

provides a model for the flow in this regime.

Scaling analysis of system (14) provides useful information. Rescaling system (14) by setting $\tau = \varepsilon^{1/3} t$, $X = \varepsilon^{-1/3} x$ and $Y = \varepsilon^{2/3} y$ yields the system

$$\begin{aligned} \frac{dX}{d\tau} &= -Y + X^2 \,, \\ \frac{dY}{d\tau} &= 1 \,. \end{aligned} \tag{15}$$

Thus, much of the ε-dependence of system (14) is described by this scale change. Solutions of system 14 are shown in Fig. 11. The heavy line is the critical manifold $y = x^2$. There is a single trajectory that maintains a bounded distance from the critical manifold as $t \to \infty$. This trajectory divides the plane into two halves. In one half, trajectories approach the stable branch of the slow manifold as $t \to \infty$. In the other half, the trajectories leave the neighborhood of the slow manifold, with $x \to \infty$ in finite time and y remaining bounded. Consider trajectories beginning at $(-1, y_0)$. As y_0 increases towards -0.1, the solutions come close to the fold (i.e., the minimum of the parabola), and follow the right branch of the parabola for increasing distances before accelerating off to the right. Further increases in y_0 yield solutions that again follow the right branch of the parabola, but then jump off the parabola on the left side (decreasing x); these trajectories then converge to the left branch of the parabola. As y_0 is increased still further, the distance that these orbits track the right branch of the parabola decreases, until finally the orbits are simply reversing their horizontal direction in the vicinity of the minimum of the parabola. Larger values of y_0 give the solutions that converge to the left branch of the parabola from the left. This qualitative picture describes the behavior of a flow near a generic fold at which trajectories on the slow manifold leave the fold.

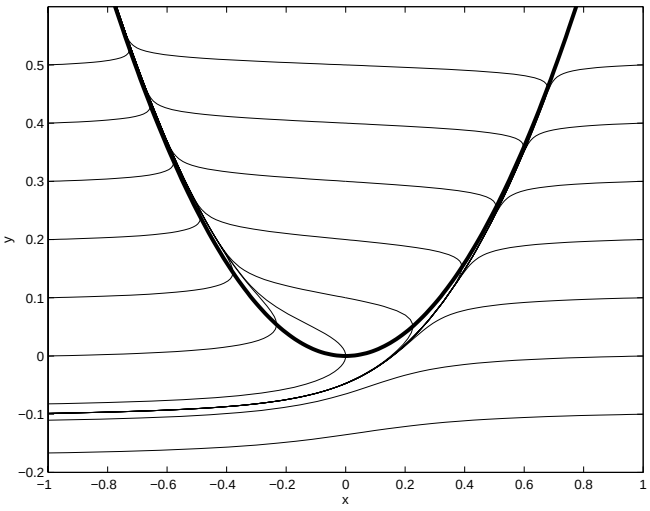

Fig. 11. Solutions to (14), the model system for the fold initiated canard, with $\varepsilon = 0.01$. The heavy line is the critical manifold $y = x^2$.

All the solutions that track the right branch of the parabola are canards. These solutions occur in a very small interval of y_0. A rigorous analysis of these observations is given by Mischenko and Rozov [1980]. These canards are also briefly discussed in Sec. 5.4 of [Arnold *et al.*, 1994]; there they are called *ducks* (i.e., *canards*) *with relaxation*. Here we give a crude estimate demonstrating that the set of initial conditions in system (14) that track the unstable slow manifold for distance 2 is a strip whose width is smaller than $\exp(-1/\varepsilon)$. The variable y increases at the constant rate ε while the variational equations show that trajectories separate from one another in the x direction at the rate $2x$. Thus, along the right-hand branch of the parabola $y = x^2$, solutions take time $1/\varepsilon$ to traverse the horizontal strip $1 < y < 2$ and they spread apart horizontally by relative amounts exceeding $\exp(-2/\varepsilon)$. Consequently, initial conditions with $x = 0$ that pass close to $(2, 4)$ on the unstable branch of the slow manifold form a strip whose width is small compared to $\exp(-1/\varepsilon)$. Thus, we expect that the saddle initiated canards of length $O(1)$ in a family of periodic orbits occur over parameter ranges that are small compared to $\exp(-1/\varepsilon)$.

In our discussion of system (14), we have considered the changes in behavior within a family of

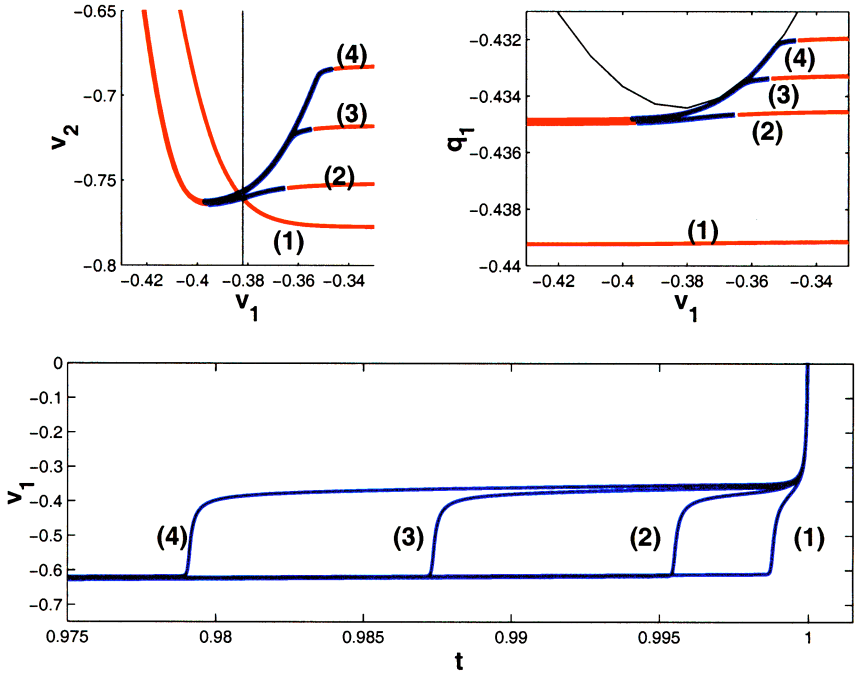

Fig. 12. A sequence of trajectories that show the formation of a fold initiated canard. The labeled curves are small parts of larger periodic orbits; we only show the region of each plot that is relevant to the formation of canards. The phase of each orbit has been chosen so that the large jump in v_1 occurs at $t \approx 1$. Orbit (1) does not have a canard. Orbits (2), (3) and (4) have canards, and the part of the orbit that tracks the slow manifold is successively longer in each.

solutions parametrized by an initial condition. In this family we see two separate asymptotic behaviors, separated by a special solution. In our numerical computation of solutions to (5), we are not varying initial conditions. We follow a family of periodic orbits. Some periodic orbits within the family may approach a fold in the critical manifold and result in fold initiated canards within the family. We have indeed found numerous examples of this; we show two of them here. However, as the canard of the periodic orbit approaches the equivalent of the special solution that separates the asymptotic behaviors in (14), the canard does not become arbitrarily long. We see in our computations that the canard eventually reaches another fold in the slow manifold, resulting in further complications and possibly additional canards. The two examples discussed below show fold initiated canards observed in our system of two coupled oscillators corresponding to the two sides of the special separating solution.

6.2.1. *Fold initiated canard (first example)*

Figure 12 shows details of four orbits from a family of periodic orbits in which a canard forms as the parameter σ_2 is varied. The orbit labeled (1) makes a fast transition that comes "close" to the slow manifold; this can be seen in the plot of v_1 versus t in Fig. 12, where v_1 jumps up at about $t = 0.998$, slows a bit when v_1 is near -0.4, and then jumps rapidly near $t = 1$. If we could watch a movie of this solution in the (v_1, v_2) plane, we would see that there is a region of the phase plane that is close to a saddle-node bifurcation. Orbit (1) is influenced by this region, but its speed does not slow down to $O(\varepsilon)$.

Orbits (2)–(4), however, do come close enough to the saddle-node region to slow down to $O(\varepsilon)$. Orbit (2) has a small canard, and in (3) and (4) the canard tracks the unstable part of the slow manifold for successively longer times. In our (v_1, v_2) movie, we would see the trajectory come close to the saddle-node point. While the trajectory lingers here, the saddle-node bifurcation takes place, and the trajectory remains near the *saddle* born in this bifurcation. The time that it stays near the saddle increases from orbit (2) to orbit (4). When the trajectory leaves the saddle, it does so by jumping *away* from the node, along the unstable manifold of the saddle in the fast (v_1, v_2) subsystem.

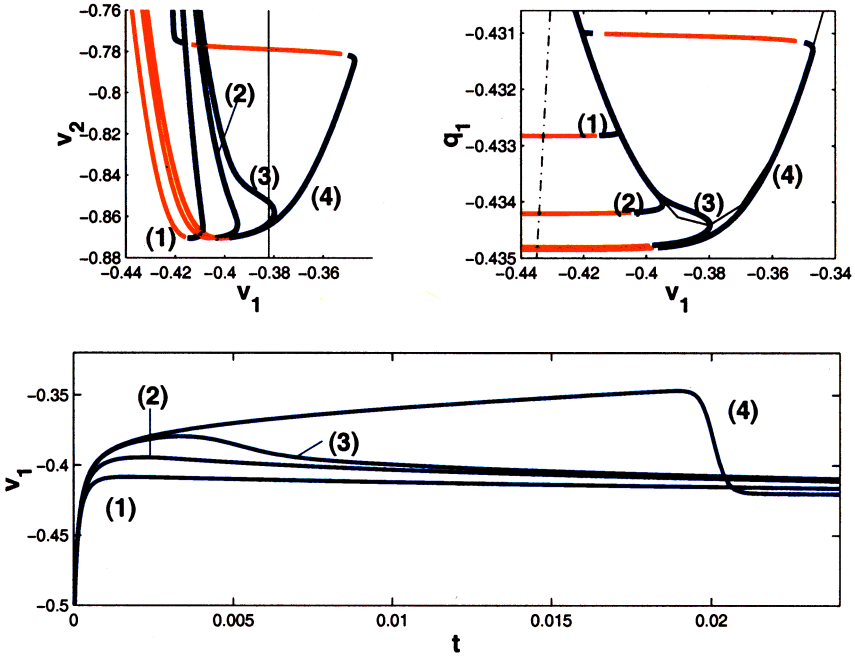

Fig. 13. A sequence of trajectories that show the formation of a fold initiated canard. The labeled curves are small parts of larger periodic orbits; we only show the region of each plot that is relevant to the formation of canards. The phase of each orbit has been chosen so that they are all making approximately the same fast transition at $t = 0$. Orbits (1) and (2) do not have canards, but the fast transition of (2) ends near the fold. The fast transition of (3) ends very close to the fold and shows the beginning of a canard. Orbit (4) shows a significant canard, in which the orbit tracks the unstable part of the slow manifold out to $t \approx 0.02$.

6.2.2. *Fold initiated canard (second example)*

Figure 13 also shows the formation of a fold initiated canard which exhibits different behavior in the phase plane of the fast subsystem. First consider orbit (1). In our (v_1, v_2) movie, we would see the trajectory get drawn into a stable node. There is a nearby saddle, but once the orbit is close to the node and we enter the slow regime, the saddle and node move apart.

In orbit (2) of Fig. 13, the trajectory gets drawn into the stable node, but now the saddle is very close. A saddle-node bifurcation is imminent. In orbits (3) and (4), the trajectory is drawn into a saddle-node point (or at least something that is extremely close to a saddle-node point), where it slows down to $O(\varepsilon)$. The saddle-node bifurcation takes place while the trajectory is nearby, and the trajectory stays near the saddle for a longer time. Orbit (3) stays near the saddle only a moderate time, while orbit (4) remains near it significantly longer. When the trajectories leave the saddle, they jump *back* to the stable node.

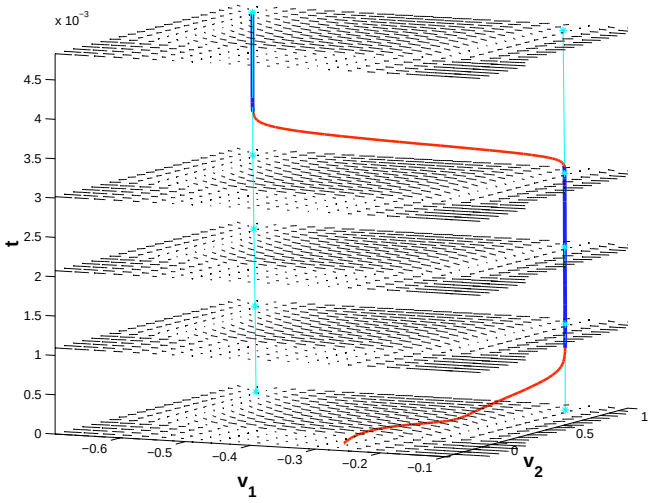

Fig. 14. A saddle initiated canard. The trajectory remains near the saddle from $t \approx 1 \times 10^{-3}$ to $t \approx 3 \times 10^{-3}$. The layers show the directions field of the fast subsystem.

6.3. *Saddle initiated canards*

A saddle initiated canard results from a fast transition being close to the stable manifold of a saddle in the fast subsystem. In the singular limit $\varepsilon = 0$, the frozen system has a normally

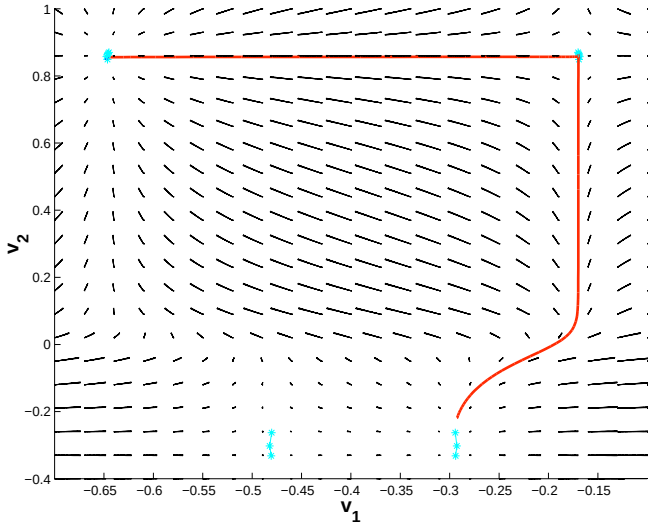

Fig. 15. A saddle initiated canard. This is the same plot as Fig. 14, but viewed from above, looking down on the (v_1, v_2) plane.

hyperbolic invariant manifold of equilibria that are saddles in the fast subsystem. Fenichel [1979] studied the persistence of normally hyperbolic manifolds and introduced coordinate systems that give normal forms for the transverse dynamics along these manifolds. Ilyashenko *et al.* [to appear] proved that C^r coordinate transformations reduce a generic three-dimensional system with one slow and two fast variables to a system of the form

$$\begin{aligned} \dot{x} &= a(z)x\,, \\ \dot{y} &= -b(z)y\,, \\ \dot{z} &= \varepsilon \end{aligned} \tag{16}$$

with a and b smooth functions of the slow variable z. Further information that is relevant to the stability of periodic orbits containing saddle initiated canards is contained in the *Exchange Lemma* of [Jones & Kopell, 1994].

An example of a saddle initiated canard is shown in Fig. 14. The three axes in this plot are v_1, v_2 and t. This is a plot of the region labeled B' in the solution discussed in Sec. 5.2, and shown in Fig. 6. At several values of t, a direction field of the phase plane of the fast subsystem is plotted. We clearly see the fast transition (from $t = 0$ to $t \approx 1 \times 10^{-3}$) that encounters a saddle in the fast subsystem. The orbit stays close to this saddle from $t \approx 1 \times 10^{-3}$ to $t \approx 3 \times 10^{-3}$. It then leaves the saddle and makes a fast transition to a stable node. The same plot, but viewed from above looking down the t axis, is shown in Fig. 15.

7. Discussion

We have shown that even the simplest singularly perturbed systems arising from neurobiology have complex dynamical behavior. We have studied a model system for reciprocal inhibition of two neurons with two fast and two slow variables. This model produces solutions containing many subtle features that span time scales. In particular, families of periodic orbits in this system encounter canards, trajectory segments that follow unstable portions of the slow manifold. There are several ways in which canards form, corresponding to different bifurcations in the singular limit of the system. We have displayed four of these: two types of "classical" canards corresponding to Hopf bifurcations and folded saddles, fold initiated canards corresponding to systems with two saddle-node points and a separatrix joining them, and saddle initiated canards in which the separatrix of a saddle-node point flows to a saddle point. Individual periodic orbits may contain several canards. We described an asymmetric periodic orbit in Sec. 5.2 that contains one fold initiated canard and two saddle initiated canards.

Our numerical study is incomplete in two fundamental respects. First, we have not addressed the stability of the periodic orbit described in Sec. 5.2. As we demonstrated in Sec. 2, the inability of numerical integration algorithms to converge to solutions with canards does not imply that these solutions are unstable. Numerical integration algorithms are simply unable to solve initial value problems that contain canards of substantial length. In contrast, boundary value problem solvers that use continuation methods to track solutions were able to compute complicated solutions containing multiple canards as shown in Sec. 5.2. Although the boundary value problem solver that we used (AUTO) was able to compute this orbit with multiple canards, its calculations of the Floquet multipliers seemed unreliable and thus did not provide stability information for the orbits. Subsequent work by Lust [personal communication] has indicated that more sophisticated algorithms than those used in AUTO are required to compute the multipliers accurately.

The second incomplete aspect of our numerical study is that we have not discussed

bifurcations of periodic orbits in this singularly perturbed system. AUTO computes one parameter families of orbits with one varying parameter in the system, but the bifurcation diagrams and information about Floquet multipliers produced by AUTO are inadequate to determine the types of bifurcations encountered within these families. Singularly perturbation theory does not yet provide foundations for such a study either. There has been little work describing the bifurcations of periodic orbits in singularly perturbed systems beyond the analysis of canard formation near Hopf bifurcations. Mechanisms for the formation and evolution of canards have been described [Arnold *et al.*, 1994; Diener, 1984], but these have not been related to the bifurcations of periodic orbits in which they appear. We hope that this work will stimulate further development of such theory. Canards are common in singularly perturbed systems even if they are difficult to compute numerically.

Acknowledgments

This research was begun at the Institute for Mathematics and its Applications at the University of Minnesota. We are enormously grateful to the IMA for its hospitality, computing resources and financial support while much of this work was completed. This research of John Guckenheimer was also partially supported by grants from the National Science Foundation and the Department of Energy.

References

Benoit, E., Callot, J. L., Diener, F. & Diener, M. [1981] "Chasse au canards," *Collect. Math.* **31**, 37–119.

Arnold, V. I. [1968] "Singularities of smooth mappings," *Russ. Math. Surv.* **23**, 1–43.

Arnold, V. I., Afrajmovich, V. S., Il'yashenko, Yu. S. & Shil'nikov, L. P. [1994] *Dynamical Systems V*, Encyclopaedia of Mathematical Sciences (Springer-Verlag).

Cohen, A. H., Rossignol, S. & Grillner, S. (eds.) [1988] *Neural Computation of Rhythmic Movement in Veterbrates* (John Wiley, NY).

Diener, M. [1984] "The canard unchained or how fast/slow dynamical systems bifurcate," *Math. Intell.* **6**, 38–49.

Doedel, E. J., Champneys, A. R., Fairgrieve, T. F., Kuznetsov, Y. A., Sandstede, B. & Wang, X. [1998] *AUTO 97: Continuation and Bifurcation Software for Ordinary Differential Equations.*

Dumortier, F. & Roussarie, R. [1996] *Canard Cycles and Center Manifolds*, Memoirs of Am. Math. Soc. 577.

Eckhaus, W. [1983] "Relaxation oscillations, including a standard chase on french ducks," *Lecture Notes in Mathematics* **985**, 449–494.

Fenichel, N. [1979] "Geometric singular perturbation theory," *J. Diff. Eq.* **31**, 53–98.

Guckenheimer, J. & Holmes, P. [1983] *Nonlinear Oscillations, Dynamical Systems and Bifurcations of Vector Fields*, Applied Mathematical Sciences, Vol. 42 (Springer).

Guckenheimer, J. & Khibnik, A. [1997] "Torus maps from weak coupling of strong resonances," preprint, Cornell University.

Guckenheimer, J. & Rowat, P. [1997] "Dynamical systems analyses of real neuronal networks," eds. Stein, P., Grillner, S. & Selverston, A. *Neurons, Networks and Motor Behavior* (MIT Press), pp. 151–164.

Hodgkin, A. L. & Huxley, A. F. [1952] "A quantitative description of membrane current and its application to conduction in nerve," *J. Physiol.* **117**, 1373–1383.

Ilyashenko, Y., Shcherbakov, A. & Yakovenko, S., to appear.

Jones, C. K. R. T. [1994] "Geometric singular perturbation theory," ed. Johnson, R. *et al.*, *Dynamical System, Montecatini Terme, Lecture Notes in Mathematics*, Vol. 1609 (Springer-Verlag).

Jones, C. K. R. T. & Kopell, N. [1994] "Tracking invariant manifolds with differential forms in singularly perturbed systems," *J. Diff. Eqs.* **108**, 64–88.

Kevorkian, J. & Cole, J. D. [1981] *Perturbation Methods in Applied Mathematics* (Springer-Verlag).

Lust, K., personal communication.

Mischenko, E. F. & Rozov, N. Kh. [1980] *Differential Equations with Small Parameters and Relaxation Oscillations* (Plenum Press).

Nadim, F., Olsen, O. H., De Schutter, E. & R. L. Calabrese [1995a] Modeling the leech heartbeat elemental oscillator I. Interactions of intrinsic and synaptic currents," *J. Comput. Neurosci.* **2**, 215–235.

Olsen, O. H., Nadim, F. & Calabrese, R. L. [1995] "Modeling the leech heartbeat elemental oscillator II. Exploring the parameter space," *J. Comput. Neurosci.* **2**, 237–257.

Rowat, P. F. & Selverston, A. I. [1993] "Modeling the gastric mill central pattern generator of the lobster with a relaxation-oscillator network," *J. Neurophysiol.* **70**(3), 1030–1053.

Skinner, F. K., Kopell, N. & Marder, E. [1994] "Mechanisms for oscillation and frequency control in reciprocally inhibitory model neural networks," *J. Comput. Neurosci.* **1**, 69–87.

Wang, X. J. & Rinzel, J. [1992] "Alternating and synchronous rhythms in reciprocally inhibitory model neurons," *Neural Comput.* **4**, 84–97.